

# MRI and pathological features of Rathke cleft cysts in the sellar region

SHOUSEN WANG\*, QUN NIE\*, ZHIFENG WU, JIANHE ZHANG and LIANGFENG WEI

Department of Neurosurgery, Fuzhou General Hospital, Fujian Medical University, Fuzhou, Fujian 350025, P.R. China

Received January 8, 2019; Accepted October 11, 2019

DOI: 10.3892/etm.2019.8272

**Abstract.** The aim of the present study was to investigate the MRI and pathological features of Rathke cleft cysts (RCC) in the sellar region. A total of 45 RCC cases were retrospectively analyzed. RCC size, location, intracyst nodules and general signals, as well as the posterior pituitary bright spot (PPBS) were analyzed using MRI-T1 weighted images (T1WI) and T2WI. The relationship between the presence of PPBS and histopathological features was additionally evaluated. On T1WI, there were 18 cases of isointense signal, 16 cases of hyperintense signal, 9 cases of hypointense signal, 1 case of heterogeneous signal and 1 case with a stratification effect, with isointense signal in the upper part and hyperintense signal in the lower part. On T2WI, there were 5 cases of isointense signal, 27 cases of hyperintense signal, 11 cases of hypointense signal and 1 case of the stratification effect. There were 10 cases of PPBS+ and 35 cases of PPBS-. There were no significant differences in the age, sex, cyst location and size between PPBS+ and PPBS- cases. However, PPBS+ cases had significantly lower inflammation than PPBS- cases. A total of 20 cases of intracystic nodules were identified on MRI scans, most of which exhibited T2 -hypointense signals. The shape of RCC nodules varied and there were 17 cases where the nodules were non-adherent to the cyst wall. The MRI signals of RCCs varied and most nodules were floating within cysts. Intracystic nodules are characteristic features of RCCs when observed by MRI and thus are of high diagnostic value. Most patients with RCC were also PPBS-, which may be associated with an increased inflammatory response.

## Introduction

Rathke cleft cysts (RCCs) originate from the Rathke pouch, with a prevalence rate of 4% (1). In the sellar region, RCCs can be found in any age group (2). Kim *et al* (3) reported that the age range of RCC patients was 11-68 years, with an average age of 37 years and an RCC size range of 5-40 mm (3). RCCs can be divided into symptomatic and asymptomatic types. Common symptoms of symptomatic RCCs include headache, vision loss, visual field defects and pituitary endocrine dysfunction (4). Uncommon symptoms include meningitis (5), pituitary abscess (6) and intracranial aneurysms (7). RCCs can be slow or acute in onset (7). MRI is the primary diagnostic technique for RCCs. Han *et al* (8) reported 10 cases of hypointense signals on T1 weighted images (T1WIs) and hyperintense signals on T2 weighted images (T2WIs), 6 cases of isointense signals on T1WIs and hyperintense signals on T2WIs, 8 cases of hyperintense signals on T1WIs and hyperintense signals on T2WIs, and 3 cases of hypointense signals on T1WIs and hypointense signals on T2WIs. The observation of intracystic nodules on MRI is an important diagnostic marker for RCCs (9). The incidence of intracystic nodules reported in previous studies was 9-77% (9-14). The cyst wall of RCCs is constructed from simple cuboidal epithelium or ciliated columnar epithelium, and the cyst contents include protein, cholesterol and mucopolysaccharide components (3). Benvensite *et al* (15) revealed that RCCs were occasionally associated with inflammatory responses.

The posterior pituitary exhibits hyperintense signals on MRI-T1WIs and is designated the posterior pituitary bright spot (PPBS) (13,14,16). PPBS is the imaging feature of antidiuretic hormone (ADH) in the posterior pituitary. Schreckinger *et al* (17) determined that postoperative RCC patients were more prone to diabetes insipidus. The positive rate of PPBS has also been reported in healthy populations (16) and patients with pituitary adenomas (18). However, the relationship between RCCs and PPBS has not yet been reported.

In the current study, the MRI features, including PPBS, of RCCs and their relationship with histopathological presentations were investigated. The relationship between the PPBS and inflammatory responses was also analyzed.

## Materials and methods

**Patients.** The current study was performed retrospectively. The sample size can be estimated according to the following

---

*Correspondence to:* Dr Shousen Wang, Department of Neurosurgery, Fuzhou General Hospital, Fujian Medical University, 156 Xihuanbei Road, Fuzhou, Fujian 350025, P.R. China  
E-mail: wangss1965@126.com

\*Contributed equally

**Key words:** Rathke cleft cyst, MRI, intracyst nodule, posterior pituitary bright spot, histopathology, inflammatory infiltration

formula:  $n = Z^2 \times [P \times (1-P)] / E^2$ , where  $n$  is the sample size,  $Z$  is the statistical value and  $E$  is the error. When the confidence is 95%,  $Z = 1.96$ ;  $P$  represents the incidence of PPBS- in the normal population, which is 4.1% according to the latest literature (19).  $E$  was set to 10% in the current study. RCC patients from January 1st 2010 to January 1st 2016 were enrolled in this retrospective study. All patients underwent RCC resection of the sellar region using the transsphenoidal approach.

The inclusion criteria for the current study were as follows: i) Patients pathologically diagnosed with RCC without sellar region involvement or primary endocrine diseases (such as primary hyperthyroidism and Cushing's disease caused by adrenal tumors); ii) patients did not receive radiotherapy or chemotherapy; iii) patients received surgery that was performed by the same surgeon; iv) patients had complete pre-operative and post-operative MRI data. Patients were excluded if treatment was discontinued or if they did not attend follow-up after surgery. Written informed consent was obtained from every patient, or their legal guardian and the study was approved by the Ethics Review Board of Fujian Medical University.

**MRI parameters.** Patients received pituitary plain and enhanced MRI scans using the Siemens 3.0T (Siemens AG). T1WI (axial and sagittal) and T2WI (the axial and coronal) scans were subsequently performed. The following parameters were used for acquisition of T1WI: TSE (turbo spin echo) sequence, TR (time of repetition)=400-500 millisecond, TE (echo time)=8-15 millisecond, 3 stimulations. The following parameters were used for acquisition of T2WI: TSE sequence, TR=3000 millisecond, TE=83-98 millisecond, 2 stimulations. The scanning field of view was 180x180 mm; matrices were 320-384x240-252; the thickness of the axial scanning layer was 3.0 mm and the layer distance was 3.0 mm; the thickness of the coronal and sagittal layer was 2.5 mm and the layer distance was 2.5 mm. Three-dimensional enhanced MRI scanning was then performed. Gd-DTPA (gadolinium-diethylenetriaminepentaacetate) was used at dose of 0.2 mmol/kg body weight and the scanning parameters were the same as the aforementioned scan.

**MRI evaluation.** Pre-operative MRI scans were reviewed by a professor of neurosurgery, an associate professor of neurosurgery and an associate professor of radiology from Fuzhou General Hospital. A consensus was reached among the physicians on all diagnoses. The MRI images at 1 week before and after the operation were analyzed. The following parameters were assessed: i) Location and size of RCC: The RCC was observed on MRI-T1WI sagittal, T2WI sagittal and enhanced T1WI sagittal. The line connecting the tuberculum sellae and the dorsum sellae was used as a reference to classify the RCCs as intrasellar, intrasellar-suprasellar or purely suprasellar. In the INFINITT PACS Medical Imaging System (syngo. via software VB10; Siemens Healthineers), the maximum diameter was used to determine the RCC size. Lesions with diameter <10 mm were considered small RCCs and lesions with a diameter  $\geq 10$  mm were considered large RCCs. ii) MRI signal and intracystic nodules in the RCC: The RCC signal was observed using both the MRI-T1WI and MRI-T2WI sequence. The nodules in the RCC (nodule number, position, size and signal characteristics) were observed under multiple

MRI sequences. iii) PPBS presentations: PPBS was observed under sagittal MRI-T1WI and defined as PPBS positive (+) and PPBS negative (-).

**Surgical approach.** Patients were placed into a supine position with a neck extension of 15-20°. The right nasal approach was selected and a nasal septum incision was performed under a surgical microscope. The nasal septum mucosa was retracted and the nasal septum bone was pushed to the left side. The surgical corridor was achieved between the right mucosal membrane lining nasal septum and ethmoid vertical plate to the front of the sphenoid sinus using a nasal speculum. A grinding drill was used to remove the anterior wall of the sphenoid sinus and the sellar face, and the sellar dura was opened in an 'X' or 'T' shape. A circular scraper, tumor tweezers and an aspirator were used to gradually remove cyst tissue, using minimal force to strip the cyst wall. When the resection was satisfactory, the lesion bed was washed repeatedly.

**Histopathological examinations.** The histopathological features of 31 RCC specimens were observed. The specimens were fixed in 10% neutral formalin solution at room temperature for 12 h, sliced (3  $\mu$ m) and paraffin embedded before staining with hematoxylin and eosin (H&E) at room temperature for 5 min for each stain. Examinations were performed under a light microscope (BX51; Olympus Corporation), including analyzing the type and the extent of fibrosis of the wall epithelium, as well as the presence of inflammatory infiltrates. The number of inflammatory cells (including neutrophils, lymphocytes and macrophages) in the slide with the largest extent of infiltration was counted. Inflammation was defined as  $\geq 10$  inflammatory cells/5 fields (magnification, x100) and <10 inflammatory cells/5 fields was determined to be negative for inflammation (magnification, x100).

**Statistical analysis.** Data were analyzed using SPSS 16.0 statistical software (SPSS, Inc.). Quantitative data were expressed as the mean  $\pm$  standard deviation. Categorical data was expressed as a percentage and analyzed using  $\chi^2$  tests (including the Fisher's exactness test). Measurement data (including age and cyst size) were tested for normality and were compared using independent t-tests.  $P < 0.05$  was considered to indicate a statistically significant difference.

## Results

**Patient demographics.** A total of 45 cases were included in the current study, including 15 males and 30 females. The average age was  $43.18 \pm 14.08$  years, ranging from 13-68 years. Among the 45 cases, 18 had pre-operative headache (40.00%), 13 experienced dizziness (28.89%), 12 demonstrated visual impairment (26.67%), 3 had polydipsia (6.67%), 1 was going through menopause (2.22%), 1 was lactating (2.22%), 3 experienced fatigue (6.67%) and 8 had no symptoms, but were diagnosed based on the result of their annual medical imaging examination (17.78%). Cyst diameter ranged from 5.60-25.47 mm (mean,  $13.80 \pm 4.99$  mm). No cases of multiple RCCs were observed.

**RCC features on MRI.** RCC features were analyzed using MRI. There were 12 intrasellar RCC cases, 33 intrasellar-suprasellar

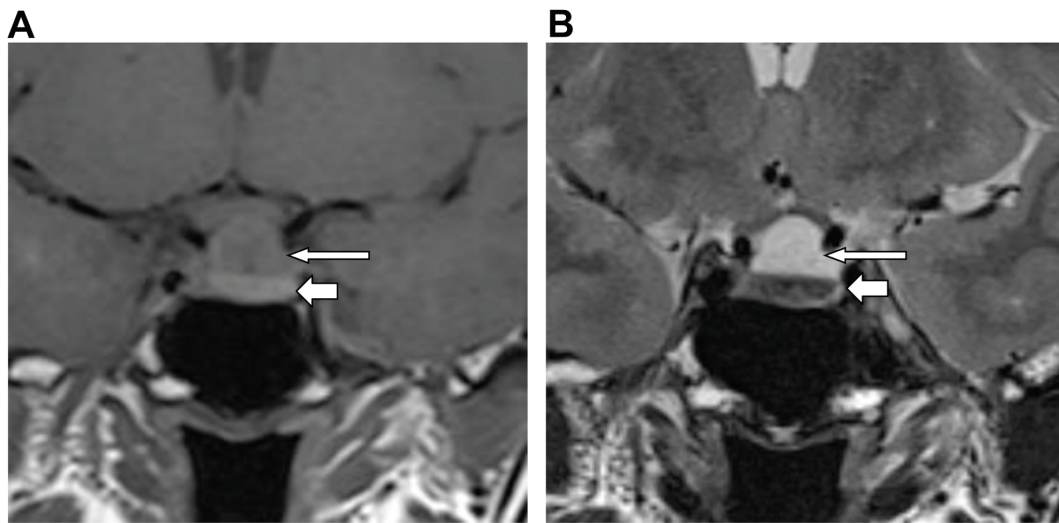


Figure 1. MRI images of a 52-year old female patient with an RCC. A stratification effect (clear boundaries of upper and lower parts) was observed. (A) Stratification effect on coronal T1WI, (B) stratification effect on coronal T2WI. RCC, Rathke cleft cyst; WI, weighted image. Long arrows show the upper parts of RCC, and short arrows show the lower parts.

cases and no purely suprasellar cases. A total of 12 cases were classified as small RCC and 33 cases were classified as large RCC. MRI-T1WI revealed 18 cases with an isointense signal, 16 cases with a hyperintense signal, 9 cases with a hypointense signal, 1 case with a heterogeneous signal and 1 case with a stratification effect [where the upper part of the RCC had an isointense signal (long arrow) and the lower part had a hyperintense signal (short arrow), with a clear border between them; Fig. 1A]. MRI-T2WI identified 5 cases with an isointense signal, 27 cases with a hyperintense signal, 11 cases with a hypointense signal, 1 case with a heterogeneous signals and 1 case of stratification (isointense signal, long arrow; hyperintense signal, short arrow; Fig. 1B).

Of the 45 cases, 20 exhibited intracystic nodules in T1WI, T2WI and T1 contrast enhanced sequences, as presented in Table I and Fig. 2. The range in nodule diameter was 1.67-9.76 (5.19±2.57) mm and the corresponding RCC diameter was 7.06-20.12 (12.65±3.07) mm, with the figures in brackets presenting the mean ± standard deviation. Of the intracystic nodules of RCCs, 3 cases exhibited hyperintense signals on T1WI, 5 cases had hypointense signals on T1WI, 13 cases had hypointense signals on T2WI, 4 cases had hypointense signal in the enhanced sequence and 2 cases had multiple nodules (as indicated by white arrows in Fig. 2F and G). There were no nodules with hyperintense signals on T2WI. The nodules were mostly of a round shape; however some displayed oval and irregular shapes and 1 case exhibited concentric rings (indicated by a white arrow in Fig. 2H). Three cases displayed intracystic nodules adherent to the cyst wall and the intracystic nodules in 17 cases were non-adherent. Several intracystic nodules were located at the center of the RCC (as indicated by white arrows in Fig. 2E and H), or in the lower, posterior or anterior parts of the RCC (as indicated by white arrows in Fig. 2A-D, F and G). These results indicated that RCCs have various signal intensities on MRI and that intracystic nodules also have various shapes and signal intensities on MRI. It is worth noting that the nodules observed through MRI were not always identified during surgery. This implies that some of the

observed nodules could be real or could be artifact created by the MRI (Fig. 3A-H).

**PPBS.** To determine the PPBS positive incidence in RCC patients, the MRI-T1WI of the 45 RCC patients were analyzed. Among the 45 RCC cases, PPBS was identified in only 10 cases. PPBS appeared in linear, triangular, crescent and bilinear shapes in the sagittal view and were located at the posterior part of the sella turcica, in contact with the dorsum sellae (Fig. 4A-F). These results indicated that the incidence of positive PPBS in RCC patients was low.

**Histopathological findings.** To observe the histopathological features of RCC, H&E staining was performed. Among the 31 pathological specimens, 12 cases exhibited cyst wall epithelium, including 4 cases of monolayer cube epithelium (as indicated by the white arrow in Fig. 5A), 7 cases displayed pseudostratified ciliated columnar epithelium and 1 case displayed ciliated columnar epithelium and squamous metaplasia (as indicated by the white arrows in Fig. 5B). Of the 25 cases with cyst content, 17 cases presented pink staining on H&E, 4 cases exhibited blue staining (as indicated by the white arrow in Fig. 5C) and 4 cases had both pink and blue staining (Fig. 5D). The arrows in Fig. 5D indicate inflammatory cell infiltrates (mainly mononuclear cells). In the tissue sections of RCC specimens with blue staining, the contents of the cysts were diverse. The size and coloration of protein bodies were highly variable and some even exhibited hyaline degeneration. No cholesterol crystals were identified. A total of 14 cases displayed inflammatory responses (Fig. 5E). The arrows in Fig. 5E show numerous pink stained protein globules in the cyst fluid. There were numerous lymphoid cells and some eosinophils in the anterior pituitary gland.

**Relationship of PPBS with age, sex, RCC location and size.** According to the presence of PPBS on MRI, patients were divided into the PPBS+ group (n=10) and the PPBS- group (n=35). The differences in age, sex, RCC location and size of

Table I. Intracystic nodules and RCC content from surgery in 20 RCC cases.

Case	Nodular signals	Nodular shape and position	Description of RCC content
1	T2 low signal	Posterior lower region of the RCC, oval, adherent to the cyst wall	Milky white mucus containing brown granules
2	T2 low signal	Right lower region of the RCC, oval, not adherent to the cyst wall	White jelly
3	High signal nodules & scattered low signal small nodules in T1	Small nodules scattered; large nodules located in the rear of the RCC, not adherent to the cyst wall, irregularly shaped	Gray and white jelly
4	Circular low signal small nodule in enhanced coronal T1WI	Centered	Thin transparent mucus
5	T1 low signal	Circular and centered	White jelly
6	Enhanced sagittal low signal	Circular and centered	Milky white jelly
7	T2 low signal of small nodules	2 circular nodules in the lower region of the RCC	Milky white jelly
8	T1 low signal, T2 low signal	Circular non-adherent nodules in the right lower region of the RCC	Milky white sticky mucus
9	T2 low signal nodules	Circular non-adherent nodules in the back region of the RCC	Gray mucus
10	T1 and T1 enhance low signal strip nodules	Irregular, front	Transparent thin mucus
11	T2 low signal nodules in the lower part	Oval, non-adherent	Yellow jelly
12	T1 high signal, T2 low signal nodules	Irregular, bottom, adherent to the cyst wall	Clear liquid and yellow solid matter
13	T2 low signal nodules	Irregular, bottom, non-adherent	Yellow-green sticky mucus
14	T1 low signal nodules	Irregular, bottom, non-adherent	Transparent liquid and jelly-like coagulum
15	T2 low signal nodules	Oval, back	Gray mucus and brown jelly-like granules
16	T2 low signal nodules	Circular, centered	Gray jelly-like material containing granules
17	T2 low signal nodules and T1 enhanced low signal	T2 round in coronal section, T1 target-like in midline sagittal section	Egg white mucus containing brown semi-solid granules
18	T1 high signal, T2 low signal of irregular nodules	Irregular	Egg white mucus containing brown solid granules
19	T1 low signal nodules	Irregular, scattered	Viscous liquid containing granules
20	T2 low signal nodules	Round, bottom right region of the RCC	Egg white mucus

RCC, Rathke cleft cyst.

cysts between the two groups were analyzed. As presented in Table II, of the 45 RCC cases, there were 15 males with 2 cases of PPBS+ and 13 cases of PPBS-. Of the 30 female cases, 8 cases of PPBS+ and 24 cases of PPBS- were identified. No significant differences were identified between the sex of the PPBS+ and PPBS- patients. In the PPBS+ and PPBS- groups, the average ages were 42.00±16.65 years and 43.51±13.51 years, respectively. No significant differences between the ages of the two groups were identified. Similarly, there were no significant differences in RCC location or size of cysts between the two groups. These results suggested that

the presence of PPBS was not associated with sex, age, RCC size or RCC location.

*Relationship of PPBS and inflammatory responses.* The relationship between PPBS status and the inflammatory response was analyzed. Among the 31 patients with histopathological specimens, 10 had PPBS+. Among the 10 cases with PPBS+, 2 (20%) had inflammatory responses. There were 21 cases of PPBS- and among them, 14 (66.7%) had inflammatory responses. The PPBS+ cases had significantly lower inflammatory responses than the PPBS- cases ( $P<0.05$ ;

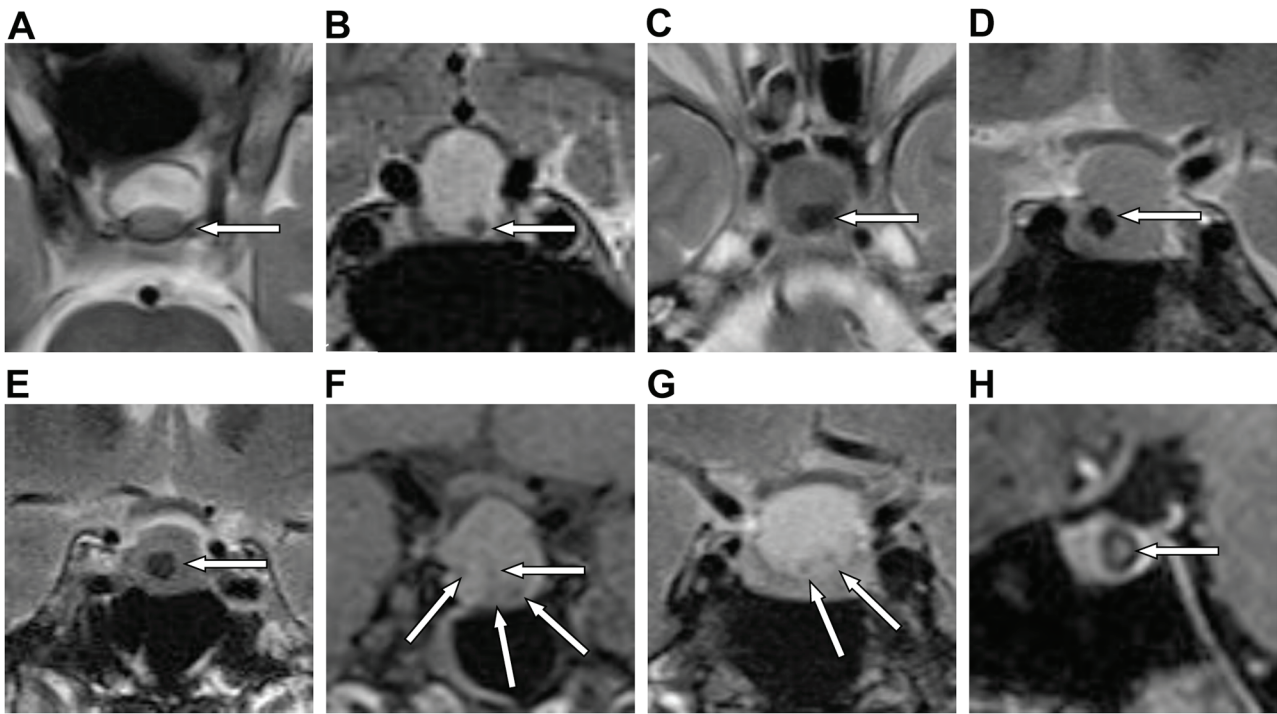


Figure 2. RCC intracystic nodules observed using MRI. Case numbers correspond with Table I. (A) Axial T2WI of case 1. An oval nodule at the back of the cyst was observed (arrow). (B) Coronal T2WI of case 20: A small nodule that adhered to the left lower wall was observed (arrow). (C) Axial T2WI of case 15: One adherent nodule was observed (arrow). (D) Coronal T2WI of case 2: A floating nodule in the right lower section was observed (arrow). (E) Coronal T2WI of case 16: An intracystic nodule in the center was observed (arrow). (F) Coronal T1WI of case 19: Multiple small scattered nodules were observed (arrows). (G) Coronal T2WI of case 8: Multiple scattered nodules were observed (arrows). (H) Enhanced sagittal T1WI of case 17: A nodule in the center with concentric rings (a target-like pattern) was observed (arrow). RCC, Rathke cleft cyst; WI, weighted image.

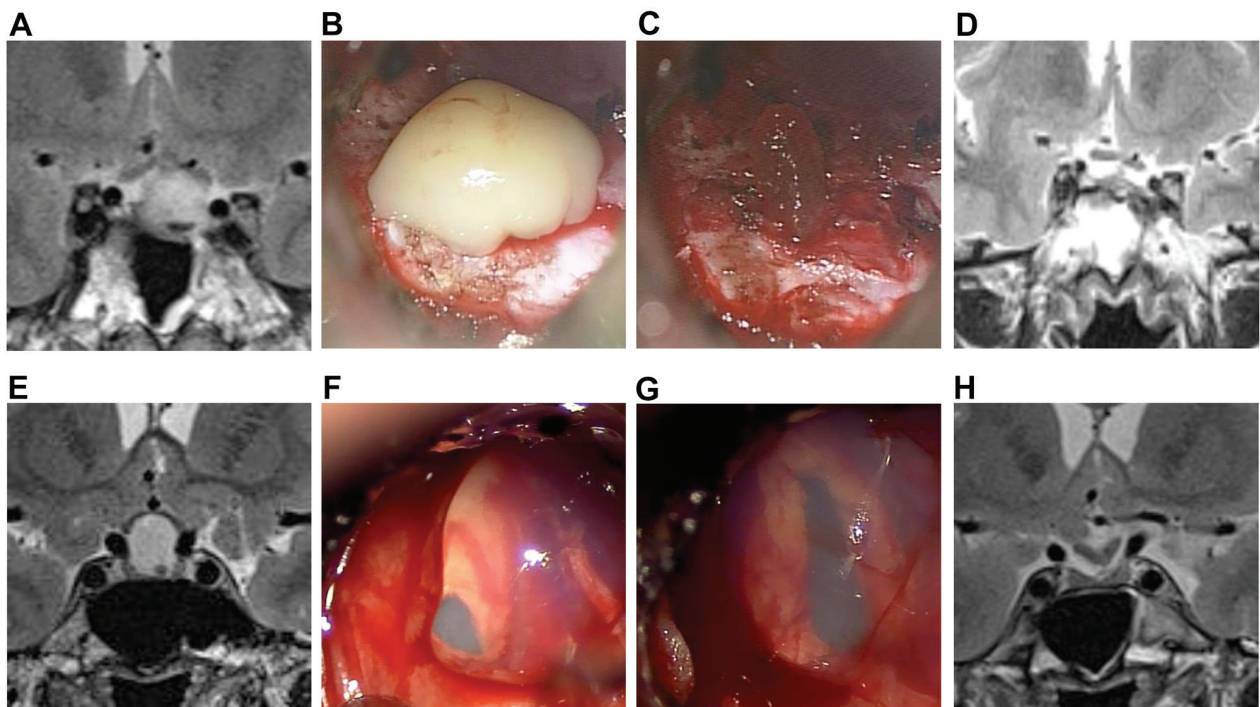


Figure 3. MRI and intra-operative images from two RCC cases. (A) The coronal T2WI image is presented. A crescent-shaped nodule with hypointense signals in the lower section of the RCC from the first patient was observed. (B) An intra-operative image of the transsphenoidal surgery of the first RCC patient. The milky white fluid flowed out of the cyst after the dura mater was cut open. (C) An intra-operative picture of the last contents of the fluid from the RCC observed in (B). The final content consisted of a small amount of brown intracystic nodules. (D) A post-operative MRI-T2WI scan is presented from this patient. The RCC and its intracystic nodules were not observed. (E) A circular-like nodule with hypointense signals was observed in the lower part of the RCC of another patient. (F) An intra-operative picture during transsphenoidal surgery on the second patient. Liquid-egg-white-like fluid flowed out of the cyst after the dura mater was cut open. (G) An intra-operative picture showing that the last contents overflowing from the RCC from (F) were a slightly thicker liquid-egg-white-like fluid. No obvious solid or semi-solid nodules were observed. (H) A post-operative MRI-T2WI images is presented from the second patient. The RCC and its intracystic nodules were not observed. RCC, Rathke cleft cyst; WI, weighted image.

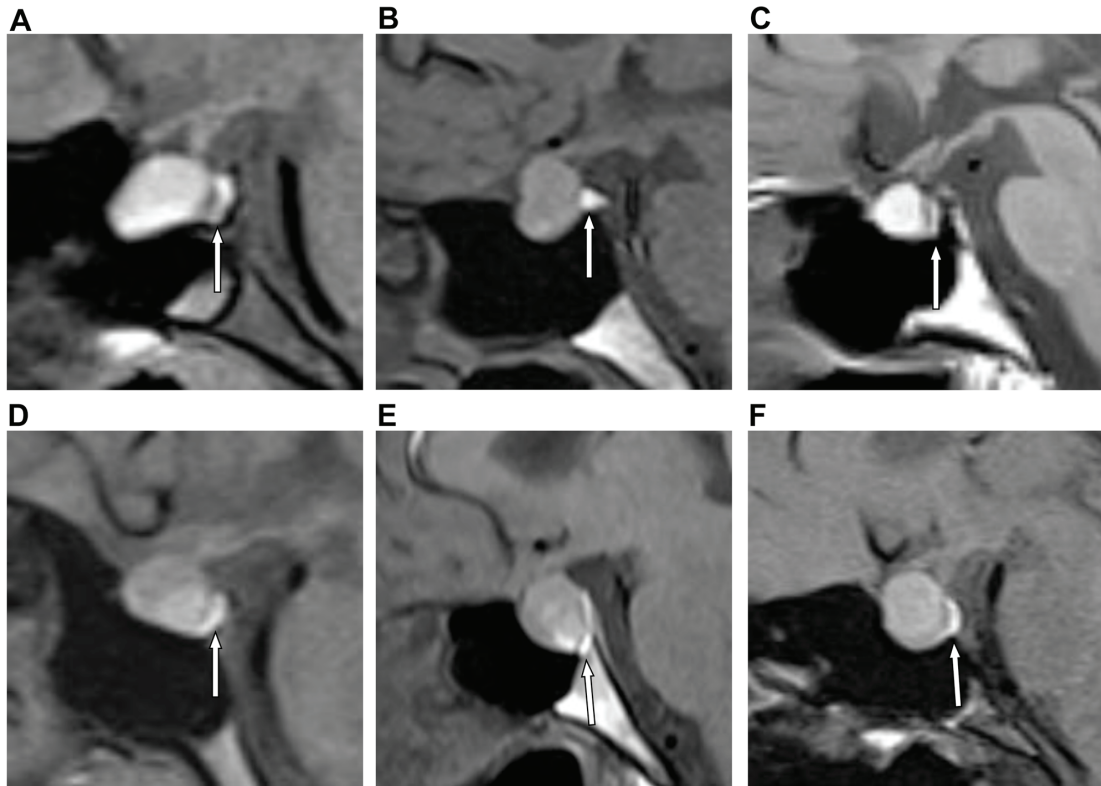


Figure 4. Shape of the PPBS (arrows) in the sagittal MRI-T1W1s of different RCC cases. (A) A 28 year old female RCC patient with an oval shaped PPBS. (B) A 38 year old female RCC patient with a triangular shaped PPBS. (C) A 54 year old female RCC patient with a linear shaped PPBS. (D) A 20 year old female RCC patient with a long strip shaped PPBS. (E) A 35 year old male RCC patient with a bilinear shaped PPBS. (F) A 42 year old female RCC patient with a crescent shaped PPBS. PPBS, posterior pituitary bright spot; RCC, Rathke cleft cyst; WI, weighted image.

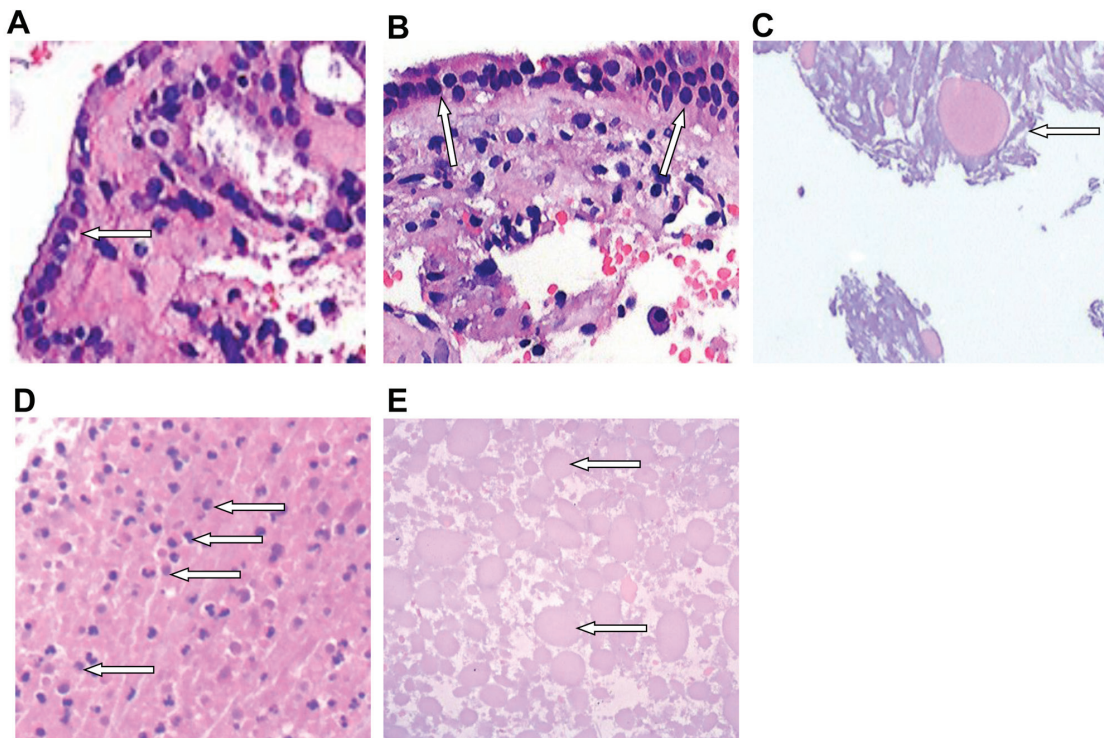


Figure 5. Histopathological presentations of different RCC cases (hematoxylin and eosin staining; magnification, x200). All images were taken using identical microscopy conditions. The different backgrounds suggest individual differences in the composition of the proteins in the cyst fluid. (A) A pathological specimen from a 67 year old male RCC patient. The arrow indicates a single-layer cubic wall epithelium. (B) A pathological specimen from a 54 year old female RCC patient. The arrows indicate a ciliated columnar epithelium and suspected squamous metaplasia. (C) A pathological specimen from a 55 year old male RCC patient. The arrow shows blue stained cyst fluid and pink stained protein globules. (D) A pathological specimen from a 47 year old male RCC patient. The arrows indicate inflammatory cell infiltrates (mainly mononuclear cells). (E) A pathological specimen from a 28 year old female RCC patient. The arrows show numerous pink stained protein globules in the cyst fluid. RCC, Rathke cleft cyst.

Table II. Association between PPBS and age, sex, cyst location and RCC size.

Variable	PPBS+ (n=10)	PPBS- (n=35)	P-value
Age, years	42±16.65	43.51±13.51	0.363
Sex			0.456
Male	2	13	
Female	8	22	
Size of cysts, mm	11.18±2.63	14.55±5.27	0.137
Cyst locations			1.000
Intrasellar	3	9	
Intrasellar-suprasellar	7	26	

Qualitative data (sex and cyst location) were compared using  $\chi^2$  tests (including Fisher exact method). Measurement data (age and cyst size) were tested for normality and were compared using independent t-tests.

Table III). Thus, the data demonstrated that the inflammatory response may be associated with the presence of PPBS.

## Discussion

In the present study, it was demonstrated that most RCCs have T1-hyperintense signal with varying signal intensity. Different patients may exhibit hyper-, iso- or hypo-intense signals on the same sequence of MRI. A stratification effect is observed in a rare number of cases. In the present study, one case presented with the stratification effect, revealing a fake 'liquid-liquid level'. This may be due to material deposition within the intracystic contents. Different components and materials may exhibit different signals on MRI. To the best of our knowledge, the present study is the first to analyze the rate of PPBS on MRI in RCC patients. The low rate of PPBS on MRI scans was also revealed to have a potential relationship with the inflammatory response exhibited by RCC patients.

According to sample size calculation, at least 16 RCC cases ( $n=1.962 \times 0.041 \times 0.959 / 0.12 = 16$ ) are required to obtain solid conclusions regarding PPBS- in RCC patients. In the present study, the 45 cases included were sufficient to reach a conclusion. Of the 45 cases, 20 had intracystic nodules, accounting for 44.44% of all RCCs. Most of the nodules were not adherent to the cyst wall. Whether the nodules are adherent to the cyst wall may be associated with the maturity of the nodules. It is hypothesized that when a nodule matures and solidifies, it easily sinks and adheres to the posterior or lower wall. In the present study, it was determined that multiple nodules may occur in one RCC, and the nodular shape may be round, oval or irregular. In the current study, there was a target-like nodule, which may be of specific value for preoperative diagnosis. It is also worth commenting that among the 20 nodular cases identified by MRI, surgery could only distinguish solid nodules in 6 of the cases and most were mucus-like or jelly-like nodules. The formation of intracystic nodules may be due to the accumulation and solidification of protein material within the cyst. Different MRI pulse sequences (repeats of the same scans or

Table III. Association between PPBS and inflammation status in RCCs.

Pathology groups	PPBS+	PPBS-	P-value (two sided)	P-value (single sided)
Inflammatory response	2	14	0.023	0.019
No inflammatory response	8	7		

Inflammatory response was considered positive when the inflammatory cells (the combined number of neutrophils, lymphocytes and macrophages)  $\geq 10$  cells/5 high magnification fields (high-power field,  $\times 100$ ). The Fisher exact test was used for statistical analysis. PPBS, posterior pituitary bright spot.

different scans), may reveal immature nodules. In the present study, nodules with hypointensity signals on T2WI were the most frequently observed, followed by nodules with hypointensity signals on T1WI. Hyperintensity signals on T1WI were rare and no hyperintensity signals on T2WI were identified.

Of the 45 patients, 10 were PPBS+, with a positive rate of 22.22%. It has been reported that the PPBS positive rate is 52-100% in the general population (16) and 79.7% in patients with pituitary adenoma (18). Furthermore, the PPBS positive rate has been demonstrated to be significantly lower in RCC patients compared with that in normal individuals (16), suggesting that the cyst has an effect on the posterior pituitary and pituitary stalk. Additionally, it has been reported that inflammatory responses are present within certain cases of RCC (6,20). The current study revealed that the PPBS+ rate was significantly lower in RCC patients with inflammatory responses than those without. The low PPBS positive rate in RCC may be associated with RCC-induced inflammatory responses. It is speculated that the inflammatory responses to RCCs can affect the pituitary stalk and the posterior pituitary, leading to a decrease in the transport and storage of ADH. This results in insufficient storage of ADH in the posterior pituitary, which may cause irreversible damage.

According to the characteristics of RCC images, RCCs can be differentiated from craniopharyngiomas, arachnoid cysts, abscesses and mucoceles. Although craniopharyngioma can exhibit significant cystic changes, parenchyma tissue is always present. The cystic wall and parenchyma reveal a significant enhancement effect on enhanced MRI. Furthermore, the vast majority of craniopharyngiomas are located above the sella turcica, rather than in the pituitary fossa (21). The MRI signal of an arachnoid cyst in the sellar region is consistent with that of cerebrospinal fluid. Arachnoid cysts are located outside the pituitary, which differentiates them from RCCs (22). Pituitary abscesses are rare and on MRI, enhancement effects are observed in the pituitary stalk, the dura mater around the pituitary and the sphenoid sinus mucosa (23). Mucoceles of the sphenoid sinus are located in the sphenoid sinus, rather than in the pituitary fossa, which are easily identified.

Despite the results obtained, the current study has limitations. Firstly, the present study was limited by the small sample size. Furthermore, the surgical procedure was written

by surgeons without the support of audio and video data, therefore the intracystic contents were described subjectively. As such, further studies are warranted.

In conclusion, the signal intensity and shape of RCC is varied on MRI. However, the intracystic nodules are featured characteristics of RCCs when investigated by MRI, which are observed in nearly 50% of RCC patients. In rare cases, RCCs demonstrated a target-like/concentric ring pattern. This shape may indicate that intracystic nodules are maturing, which is of great importance for RCC diagnosis. Inflammatory responses were observed in some RCC cases, which may affect the appearance of the PPBS on T1WI. The mechanism underlying the appearance of PPBS on T1WI with inflammatory responses is unclear and needs further investigation.

### Acknowledgements

Not applicable.

### Funding

The present study was supported by the Fujian Provincial Key Project of Science and Technology Plan (grant no. 2018Y0067).

### Availability of data and materials

The datasets used and/or analyzed during the present study are available from the corresponding author on reasonable request.

### Authors' contributions

SW conceptualized the study. QN, ZW and JZ collected the cases and the subsequent data. LW analyzed the data. SW and QN wrote the original manuscript. SW reviewed and edited the manuscript as well as acquired funding for the project.

### Ethics approval and consent to participate

All subjects gave their written informed consent for inclusion before they participated in the study. The study was conducted in accordance with the Declaration of Helsinki, and the protocol was approved by the ethics review board of Fujian Medical University.

### Patient consent for publication

Not applicable.

### Competing interests

The authors declare that they have no competing interests.

### References

1. Kuan EC, Yoo F, Chyu J, Bergsneider M and Wang MB: Treatment outcomes of Rathke's cleft cysts managed with marsupialization. *J Neurol Surg B Skull Base* 78: 112-115, 2017.
2. Lin M, Wedemeyer MA, Bradley D, Donoho DA, Fredrickson VL, Weiss MH, Carmichael JD and Zada G: Long-term surgical outcomes following transsphenoidal surgery in patients with Rathke's cleft cysts. *J Neurosurg* 130: 831-837, 2018.

3. Kim JE, Kim JH, Kim OL, Paek SH, Kim DG, Chi JG and Jung HW: Surgical treatment of symptomatic Rathke cleft cysts: Clinical features and results with special attention to recurrence. *J Neurosurg* 100: 33-40, 2004.
4. Jahangiri A, Molinaro AM, Tarapore PE, Blevins L Jr, Augustine KI, Gupta N, Kunwar S and Aghi MK: Rathke cleft cysts in pediatric patients: Presentation, surgical management and postoperative outcomes. *Neurosurg Focus* 31: E3, 2011.
5. Mrelashvili A, Braksick SA, Murphy LL, Morparia NP, Neena N and Neeraj K: Chemical meningitis: A rare presentation of Rathke's cleft cyst. *J Clin Neurosci* 21: 692-694, 2014.
6. Naama O, Gazzaz M, Boulahroud O and Elmoustarchid B: Infection of a Rathke cleft cyst: A rare cause of pituitary abscess. *Surg Infect (Larchmt)* 15: 358-360, 2014.
7. Jimbo H, Ichikawa M, Fukami S, Otsuka K, Tsurukiri J, Sunaga S and Lkeda Y: Rapid De Novo aneurysm formation after Rathke cleft cyst rupture. *World Neurosurg* 88: 690.e11-690.e16, 2016.
8. Han X and Zhao DJ: Imaging diagnosis of Rathke's cleft cyst. *J Med Imag* 20: 782-784, 2010.
9. Wang SS, Xiao DY, Yu YH, Jing JJ, Zhao L and Wang RM: Diagnostic significance of intracystic nodules on MRI in Rathke's cleft cyst. *Int J Endocrinol* 2012: 958732, 2012.
10. Binning MJ, Gottfried ON, Osborn AG and Couldwell WT: Rathke cleft cyst intracystic nodule: A characteristic magnetic resonance imaging finding. *J Neurosurg* 103: 837-840, 2005.
11. Byun WM, Kim OL and Kim D: MR imaging findings of Rathke's cleft cysts: Significance of intracystic nodules. *AJNR Am J Neuroradiol* 21: 485-488, 2000.
12. QI C and Wang N: Value of intracystic nodules on MRI to diagnosis of Rathke's cleft cyst. *Chin J Clin Neurosurg* 19: 212-214, 2014.
13. Kilday JP, Laughlin S, Urbach S, Bouffet E and Bartels U: Diabetes insipidus in pediatric germinomas of the suprasellar region: Characteristic features and significance of the pituitary bright spot. *J Neurooncol* 121: 167-175, 2015.
14. Saeki N, Hoshi S, Sunada S, Sunami K, Murai H, Kubota M, Tatsuno I, Iuchi T and Yamaura A: Correlation of high signal intensity of the pituitary stalk in macroadenoma and postoperative diabetes insipidus. *AJNR Am J Neuroradiol* 23: 822-827, 2002.
15. Benveniste RJ, King WA, Walsh J, Lee JS, Naidich TP and Post KD: Surgery for Rathke cleft cysts: Technical considerations and outcomes. *J Neurosurg* 101: 577-584, 2004.
16. Côté M, Salzman KL, Sorour M and Couldwell WT: Normal dimensions of the posterior pituitary bright spot on magnetic resonance imaging. *J Neurosurg* 120: 357-362, 2014.
17. Schreckinger M, Szerlip N and Mittal S: Diabetes insipidus following resection of pituitary tumors. *Clin Neurol Neurosurg* 115: 121-126, 2013.
18. Wang S, Lin K, Xiao D, Zhao L, Qin Y and Wei L: MR imaging analysis of posterior pituitary in patients with pituitary adenoma. *Int J Clin Exp Med* 8: 7634-7640, 2015.
19. Klyn V, Dekeyzer S, Van Eetvelde R, Roels P, Vergauwen O, Devolder P, Wiesmann M, Achten E and Nikoubashman O: Presence of the posterior pituitary bright spot sign on MRI in the general population: A comparison between 1.5 and 3T MRI and between 2D-T1 spin-echo- and 3D-T1 gradient-echo sequences. *Pituitary* 21: 379-383, 2018.
20. Ogawa Y, Watanabe M and Tominaga T: Intraparenchymal infiltration of Rathke's cleft cysts manifesting as severe neurological deficits and hypopituitarism: 2 Case reports. *BMC Res Notes* 9: 225, 2016.
21. Locatelli D, Pozzi F, Agresta G, Padovan S, Karligkiltis A and Castelnovo P: Extended endoscopic endonasal approach for suprasellar craniopharyngioma. *J Neurol Surg B Skull Base* 79: S196-S198, 2018.
22. Abbas M, Khairy S, AlWohaibi M, Aloraidi A and AlQurrashi WW: Bilateral temporal extradural hematoma on top of bilateral temporal arachnoid cyst: First case report and extensive literature review. *World Neurosurg* 115: 134-137, 2018.
23. Ifergan H, Cazeneuve N, Merenda P and Magni C: MR imaging features of a pituitary abscess: A case report. *Ann Endocrinol (Paris)* 80: 62-63, 2019.



This work is licensed under a Creative Commons Attribution-NonCommercial-NoDerivatives 4.0 International (CC BY-NC-ND 4.0) License.